Direct Observation of Amyloid Nucleation under Nanomechanical Stretching

Nitinun Varongchayakul,[†] Sara Johnson,[‡] Trina Quabili,[‡] Joseph Cappello,[§] Hamidreza Ghandehari,[§,⊥] Santiago De Jesus Solares,[¶] Wonmuk Hwang,[#,▽] and Joonil Seog[†,*]

[†]Department of Materials Science and Engineering, [‡]Fischell Department of Bioengineering, [¶]Department of Mechanical Engineering, University of Maryland, College Park, Maryland 20742, United States, [§]Department of Pharmaceutics and Pharmaceutical Chemistry [⊥]Department of Bioengineering, Utah Center for Nanomedicine, Nano Institute of Utah, University of Utah, Salt Lake City, Utah 84108, United States, [#]Departments of Biomedical Engineering and Materials Science & Engineering, Texas A&M University, College Station, Texas 77843, United States , and [▽]School of Computational Sciences, Korea Institute for Advanced Study, Seoul, 130-722 Korea

ABSTRACT Self-assembly of amyloid nanofiber is associated with both functional biological and pathological processes such as those in neurodegenerative diseases. Despite intensive studies, the stochastic nature of the process has made it difficult to elucidate a molecular mechanism for the key amyloid nucleation event. Here we investigated nucleation of the silk-elastin-like peptide (SELP) amyloid using time-lapse lateral force microscopy (LFM). By repeated scanning of a single line on a SELP-coated mica surface, we observed a sudden stepwise height increase. This corresponds to nucleation of an amyloid fiber, which subsequently grew perpendicular to the scanning direction. The lateral force profiles followed either a worm-like chain model or an exponential function, suggesting that the atomic force microscopy (AFM) tip stretches a single or multiple SELP molecules along the scanning direction. The probability of nucleation correlated with the maximum stretching force and extension, implying that stretching of SELP molecules is a key molecular event for amyloid nucleation. The mechanically induced nucleation allows for positional and directional control of amyloid assembly *in vitro,* which we demonstrate by generating single nanofibers at predetermined nucleation sites.

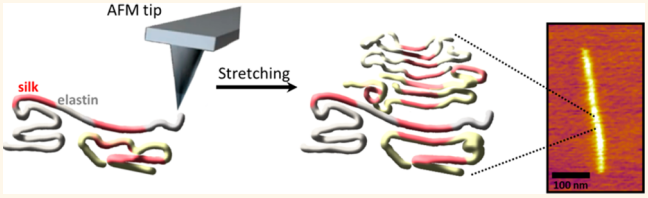

KEYWORDS: atomic force microscopy · amyloid · nucleation · silk · elastin · lateral force microscopy · sacrificial bond · self-healing · protein polymer · nanomechanics

Self-assembly of relatively long peptides is a complex process due to multiple conformational states explored by the molecule. While making dynamic transitions among these states on a rugged energy landscape,[1] the molecule can find a conformation permissible for assembly into the characteristic cross-β structure of amyloid where individual β-strands are perpendicular to the fibril axis.[2] Previous studies suggest that the ability to form an amyloid fiber is an intrinsic property of peptides in nature, so that many different peptides have been used as model systems to study amyloid fibrillogenesis.[3]

A key event in this process is the nucleation step, which is known to have a high activation energy barrier.[4] This causes the initial lag phase before growth that is influenced by various factors such as pH, ionic strength, temperature, and the presence of seeds.[5,6] Often, amorphous aggregates or protofibrils undergo conformational transition to nucleate an amyloid fiber.[7−9] Furthermore, experimental conditions can guide the dynamic equilibrium among different conformational states into nucleating species which determine molecular ordering in the resultant amyloid fibers, referred to as molecular polymorphism.[10] In addition to studies in bulk solution, amyloid formation on surfaces has been actively investigated since it may more closely mimic physiological environments such as cell membrane.[11] The surface can accelerate assembly or it may guide the growth direction.[12−18] Fundamental understanding of the effect of the substrate on the self-assembly of amyloids may also be useful for creating functional nanostructures based on substrate-directed self-assembly.[19−21] To this end, mechanistic understanding of the key nucleation event is essential.

A model amyloid peptide that has recently drawn much attention is silk-elastin-like

* Address correspondence to jseog@umd.edu.

Received for review May 8, 2013 and accepted August 29, 2013.

Published online August 29, 2013
10.1021/nn402322k

peptide polymer (SELP). It consists of alternating domains of 8 silk-like units (GAGAGS), 15 elastin-like units (GVGVP), and 1 elastin unit modified by the substitution of valine to lysine (GKGVP).[22] The proline-rich elastin unit provides high extensibility and unique thermal responsive properties of spider silk,[23] while the silk unit controls the stiffness of the hydrogel formed by SELP.[22] We have recently discovered that SELP assembles on a mica surface at an ultrafast rate with virtually no lag phase.[24] We also observed that the growth of SELP amyloid can be enhanced by nanomechanical force exerted during tapping mode imaging of atomic force microscopy (AFM).[25] Interestingly, the mechanically induced amyloid tends to grow perpendicular to the AFM scanning direction, implying that the amyloid growth direction is determined during nucleation. This novel aspect was used to simultaneously control the location of nucleation and the growth direction to create a SELP nanofiber patterned surface in 1 μm length scale.[26] However, the molecular mechanism underlying mechanically induced nucleation of SELP amyloid remains to be found.

In this work, we applied time lapse lateral force microscopy (LFM) to study the nucleation mechanisms of SELP on a mica surface in the contact mode AFM. For higher temporal resolution, the slow scan axis was disabled and a single line was continuously scanned to observe the nucleation event in real time. As the tip of the AFM scans the surface, it occasionally picks up strands of SELP and stretches them until losing contact. The stretching of SELP is followed by nucleation of a fiber growing perpendicular to the stretching direction, where the probability of nucleation is correlated strongly with the stretching force profiles. It thus appears that, mechanical stretching of a SELP provides a template on which the amyloid cross-β structure can grow. Supporting this idea, the measured dimensions of the fiber agreed well with those of our molecular model of SELP amyloid. Utilizing the mechanical induction, we were able to nucleate a single nanofiber at a prescribed location and growth direction. In addition to practical potential for positional and directional control in nanopatterning amyloid fibers, the present results may help to understand how mechanical forces alter the energy landscape and guide the conformational transition from disordered and loosely bound peptide aggregates to the paracrystalline amyloid fiber.

RESULTS AND DISCUSSION

Direct Observation of Morphological Evolution of Nuclei *in Situ*. A 40 μL aliquot of the SELP solution (5 μg/mL in distilled water) was deposited on a freshly cleaved mica disk and incubated for 30 min at room temperature. During incubation, SELP adsorbs on the mica surface, forming a SELP-coated layer (see Supporting Information, Figure 1). After incubation, the sample was washed with water three times and immediately used for AFM experiments in water. Thus, nucleation and growth of SELP fibrils is due to the assembly of surface-adsorbed molecules. While it is possible that a small fraction of the surface-adsorbed SELP molecules can redissolve into water, it is unlikely they will play any major role in nucleation since soluble SELP will not generate measured force profiles described in the following sections. The SELP was also attached to the AFM tip by physisorption in the lateral scanning mode. During time-lapse LFM scan, the normal force was maintained at ~140 pN while the lateral deflection was used to measure lateral force along the scan direction (Figure 1 inset). We also measured height profiles during LFM scan to simultaneously observe the morphological evolution of nuclei and the lateral force as a function of time.

At the beginning of the scan, there were heightened features due to the presence of amyloids that were preformed during the incubation stage (Figure 1a, arrows). Later on, multiple heightened sites appeared at different time points (Figure 1a, asterisks). A zoomed-out image of the scanned line (dotted line in Figure 1b) indicated that amyloid nanofibers grew from these locations, suggesting that increases in height during line scans correspond to nucleation events. Many previous studies show a distribution of morphologies and sizes of prefibrillar intermediates leading to amyloid fibrils, including spheroidal or toroidal high-molecular weight oligomers and low-molecular weight oligomers (dimers, trimers, *etc.*).[27,28] In our case, it is difficult to identify such prefibrillar intermediates since SELP nanofiber grows rapidly after initiation. This reflects that a mechanical force effectively accelerates conformational transition from intermediates to β-sheet fibrils. We hence call the mechanically induced increase in height followed by growth of amyloid as a "nucleation event", and the first occurrence of the increase in height as a "nucleus". As discussed below, nucleation of a nanofiber occurs in stretching events with quantitatively different force profiles, which further support heterogeneity and multiple pathways in nucleation events.

Representative profiles of the height evolution during nucleation are shown in Figure 2a (see Supporting Information Figure 2). The increase in height occurred in a stepwise manner. The smallest step size was 1.2 $\pm$ 0.2 nm (n = 7) which matches the dimension of a one β-sheet bilayer (Figure 2a).[17] There were also cases with 2.1 $\pm$ 0.1 nm (n = 7) and 3.5 $\pm$ 0.2 nm (n = 32) steps, which are approximately integer multiples of 1.1 nm and suggest that multiple β-sheet bilayers can form simultaneously within the 2-Hz time resolution of our scans (Figure 2b). The fully grown height of nuclei coincides with the height of preformed amyloid, 3.7 $\pm$ 0.2 nm (n = 7). This indicates that SELP amyloids assembled by mechanical stimuli have similar dimensions as those preformed without force.

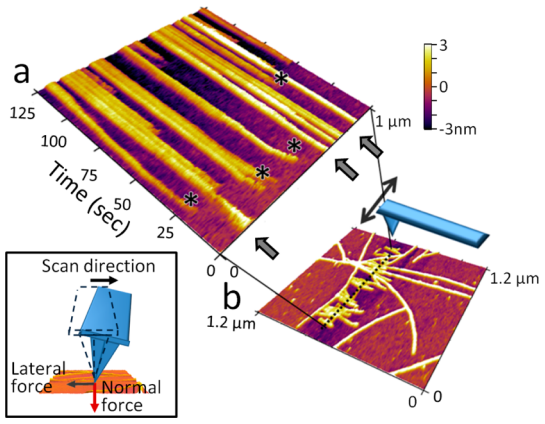

Figure 1. Time-lapse lateral force microscopy (LFM) reveals the evolution of amyloid nucleation events. (a) Height image of time-lapse LFM. An AFM tip scanned on a SELP adsorbed mica surface along a fixed scan line as a function of time. The heightened areas at $t = 0$ (arrows) are due to amyloids preformed during the incubation stage. Later, multiple heightened sites formed (asterisks). (b) Zoomed-out AFM image after the time-lapse LFM experiment. Dotted line is where the single line was repeatedly scanned. Multiple nanofibers grew approximately perpendicular to the scan line, confirming that the newly formed heightened sites were indeed the nuclei for new amyloid nanofibers. (Inset) Scheme for the LFM experiment. Torsion of the cantilever occurs in response to lateral forces while normal bending of the cantilever occurs in response to normal forces.

Vertical stacking of multiple β sheet layers in nanofilaments has been reported for a short peptide with up-right conformations.[29,30] In the case of SELP, a monomer is much larger and the resulting nanofiber has disordered elastin domains protruding on the side of the cross-β core (cf., Figure 6). The SELP filament thus likely grows with its β-sheet parallel to the mica surface, which is supported by the measured step sizes in height. The fiber also grew stepwise in width (Figure 2c). The smallest width of nuclei without correcting for the tip radius is 19 $\pm$ 2.4 nm (n = 6) (Figure 2c). The major population of nuclei shows the width of 41 $\pm$ 16 nm (n = 38), which is twice the smallest width. Sometimes, a secondary nucleation occurred right next to a primary nucleus (Figure 2c(iii)). When a sharpened tip with 2-nm radius was used to minimize the effect of the finite tip radius, the width of mature fibers was measured to be 13 $\pm$ 4 nm (n = 14) which is comparable to that of the 42-residue Alzheimer's β-amyloid (Aβ1-42).[17] This suggests that the silk unit $(GAGAGS)_8$ of SELP which is similar in size to Aβ1-40 or Aβ1-42, likely forms an amyloid core composed of a hairpin-like bilayer by folding in half.[31−33] The thickness of the SELP amyloid measured in our experiments is ~1.2 nm, which is slightly thinner. This may be because the hairpin-like folding will put one face of the β-sheet covered with glycines that do not have a protrusive side chain. β turn formation nucleates the intramolecular folding of the Aβ monomer from which subsequent assembly proceeds.[34] In our case, mature fibers contained about three β-sheet bilayers (Figure 2a), so that one or two bilayers may comprise a nucleus.

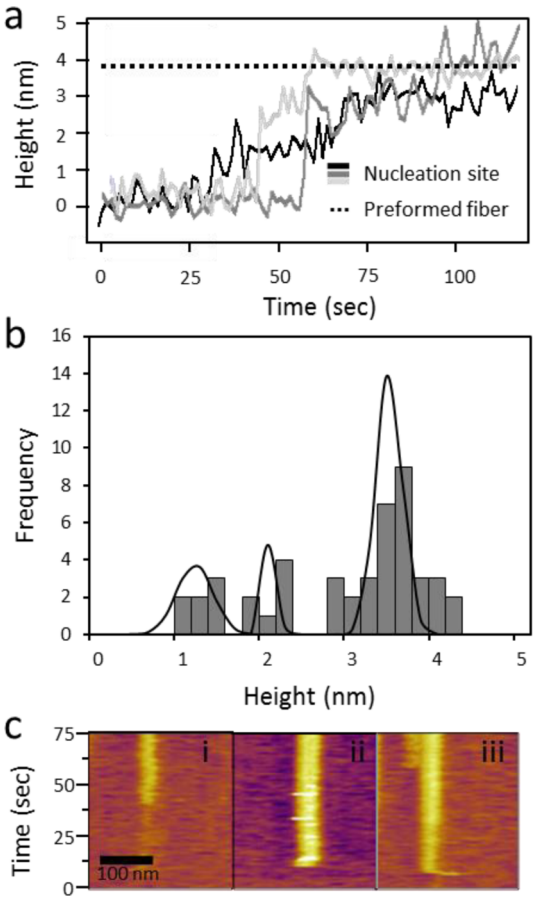

Figure 2. Stepwise increase in (a,b) height and (c) width of amyloids. (a) Height increase of amyloid nuclei as a function of time. A sudden stepwise increase in height occurred during time-lapse LFM. While individual assembly events take different step sizes, they approach the height of preformed fibers at later time points. (b) Histogram of height increases. The smallest step size is ~1.2 nm. (c) Quantized growth in the width of nuclei. (i) The smallest width of amyloid nucleus (19 $\pm$ 2.4 nm (n = 6)). (ii) The most abundant width of amyloid nucleus, which is twice the smallest width, (41 $\pm$ 16 nm (n = 38)). (iii) Secondary nucleation next to the primary nucleation site.

Promotion of Nucleation by Increased Lateral Force. To elucidate the role of force on nucleation, we compared height profiles with the corresponding lateral force profiles. The lateral force is recorded positive during trace and negative during retrace for a scan, creating a hysteretic loop. In the example shown in Figure 3, the trace and retrace of height profile shows a nucleation event at 36.5 s (Figure 3a,b) which is accompanied by the increase in lateral force during retrace (dark horizontal line in Figure 3d). After nucleation, the lateral force is slightly changed as the tip contacts the nucleus in the following traces and retraces. Figure 3e shows five consecutive scans around the time of nucleation. At 35.75 and 36.00 s, there are no significant variations in both height and lateral force profiles. At 36.25 s, the lateral force significantly increases to 800 pN, and suddenly drops while the height profile still remains flat. Subsequently at 36.50 s, a sudden increase in height appears (asterisk in Figure 3e),

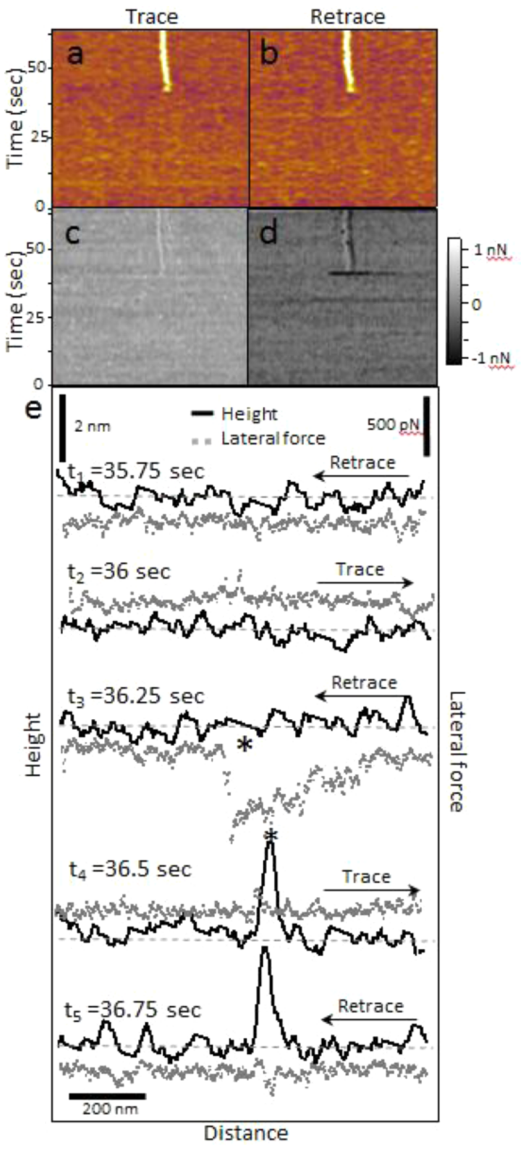

Figure 3. Increase in lateral force prior to amyloid nucleation. Trace and retrace of height (a, b) and lateral force profiles (c, d) for a single nucleation event. (e) Height and lateral force profiles at five successive time points (height profiles in black and lateral force profiles in gray). The dotted gray line shows zero lateral force and zero height. A sudden increase in the lateral force at t_3 (asterisk) is followed by a height increase in the next scan, indicating that a new nucleus (asterisk) is formed.

indicating that a nucleus is formed. The increased height is maintained in the following retrace scan (t_5 = 36.75 s) and thereafter. Thus, an increase in force profile precedes nucleation, which likely corresponds to the stretch of a SELP molecule. After nucleation, the lateral force returns to near-base level except for a mild increase at the nucleation site due to the heightened feature (Figure 3c,d). Not all increases in lateral force resulted in nucleation. However, all new nucleation events were preceded by increases in lateral force, which indicates that the latter is a necessary condition for nucleation.

We analyzed ~100 frictional force profiles that led to nucleation, and classified them into three categories: worm-like chain (WLC; Figure 4a), sawtooth (Figure 4b), and exponential (Figure 4c) profiles. We fit the WLC profile by the relation[35]

$$F(x) = \frac{k_b T}{L_p}\left(\left[\frac{1}{4\left(1-\frac{x}{L_c}\right)^2}\right] - \frac{1}{4} + \frac{x}{L_c}\right)$$

where F is lateral force along the stretching direction, k_b is Boltzmann constant, T is absolute temperature, L_c is the contour length, and L_p is the persistence length. Estimated values of the persistence and contour lengths are $L_p = 0.25 \pm 0.2$ nm and $L_c = 332 \pm 161$ nm ($n = 15$). The persistence length is close to the value of 0.4 nm from single-elastin stretching experiments.[36] We carried out single SELP stretching experiments where the molecule is pulled normal to the mica surface, which also yielded $L_p = 0.28 \pm 0.1$ nm and $L_c = 284 \pm 13$ nm ($n = 64$) (Supporting Information Figure 3). Furthermore, the contour length is comparable to the length of a fully extended SELP molecule, 295 nm (=818 residues × 0.36 nm). These suggest that in cases with WLC profiles, a single SELP molecule is stretched by the AFM's tip. The maximum stretching force level of WLC profiles was 318 ± 128 pN (n = 15). The value of L_c is slightly greater than that of a SELP molecule likely because other SELP molecules (adsorbed either to mica or to AFM tip) that hold the one being stretched may also contribute to extension.

In cases with sawtooth profiles (Figure 4b), the initial rise in force was well-fit with the WLC model, which gave $L_p = 0.21 \pm 0.2$ nm, and $L_c = 314 \pm 95$ nm (n = 55). Unlike a single WLC behavior, however, a plateau follows after the initial rise in the sawtooth profile. The average peak force in the sawtooth pattern was 218 ± 158 pN (n = 55), ranging from 133 pN to 691 pN. The average peak-to-peak distance was 33 ± 9 nm (n = 75), with the number of peaks in one pattern varying from 2 to 14. The stretching length, defined as the distance from the start of the initial WLC to where the sawtooth finishes, was 341 ± 201 nm, which is close to the contour length of SELP, again suggesting that a single SELP molecule is stretched in the sawtooth cases. The narrow distribution of peak-to-peak distance is likely due to successive unraveling of well-defined structures. Sequential detachments of multiple molecules can produce a similar profile with decreasing peak forces,[37] but in our case the maximum stretching force typically occurs at the last peak of a sawtooth profile. It is thus more likely that the sawtooth pattern originates from stretching a single SELP molecule where locally ordered domains are unfolded in a serial manner, thereby exposing hidden lengths and reducing the force level. Yet, since a single molecule is pulled, the maximum force is achieved mostly at the end of the pull. A similar sawtooth pattern was previously observed when a β-sheet secondary

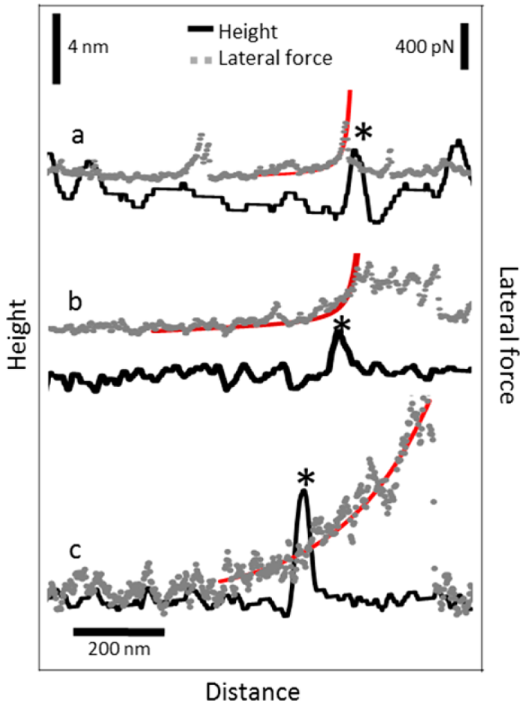

Figure 4. Three characteristic force behaviors in lateral force profiles (gray dot). (a) Worm-like chain (WLC) behavior, (b) WLC with a sawtooth pattern, and (c) exponential behavior. Nuclei are marked by asterisks in height profiles (black). WLC model (a, b) and exponential model (c) fits are shown in red.

structure on the surface is disrupted by mechanical force.[21] In their study, the unfolding force ranged from 70 to 200 pN, which is similar to that in our experiments. As discussed above, the 48-residue silk units are locally ordered and are joined by the 80-residue elastin units. The length of the elastin unit (= 80 residues × 0.36 nm = 29 nm) is very close to the average peak-to-peak distance, implying that each peak in the sawtooth pattern is caused by extension of the elastin unit while each silk unit remains folded in a hairpin-like state. The sawtooth profile may thus occur when the tip of the AFM pulls on a partially ordered SELP, whereas in the WLC profile, it is likely that the SELP molecule is in a more disordered state. The exponential profiles were identified as those that yielded an order of magnitude smaller persistence length when fit with the WLC equation. They were instead fit using the following equation.[38]

$$F(x) = F_p \exp\left(\frac{x - x_p}{D}\right)$$

where F_p is the peak force, x_p is the location of the peak, and D is the characteristic length scale for the pulling event. Fitting the data falling into the exponential profile with the WLC model produced longer L_c (512 ± 241 nm) and an order of magnitude shorter L_p (0.08 ± 0.28 nm) (n = 32), which indicates that the WLC model is inadequate. The maximum stretching force was 1011 ± 970 pN (n = 32), significantly higher than those of the WLC or sawtooth profiles. An exponential model was previously used to describe the mechanical behavior of molecular and supramolecular structures of the flagelliform protein of spider silk.[38] Flagelliform protein is rich in proline and contains highly repetitive β-spiral sequences, similar to the elastin unit of SELP. We thus hypothesize that the exponential profiles in our study originate from pulling on a network of multiple SELPs that are cross-linked by silk units through β-sheet formation, whereas elastin units provide flexible linkage between the ordered domains of the silk units. The molecular network appears to be mechanically robust since the force profile showed almost monotonic increase with relatively small drops in force during stretching. The stretching length was 482 ± 271 nm (n = 32), varying widely from 152 to 1029 nm, and it was mostly longer than the contour length of a single SELP molecule, which supports involvement of multiple molecules. The characteristic length D = 127 ± 55 nm (n = 32), can be interpreted as the distance between cross-linking points in the network. This is about 4 times longer than the length of a single elastin unit, which again suggests that the exponential behavior arises from collective response of multiple molecules, likely an oligomeric network of SELP.

Enhanced Probability of Nucleation for the Exponential Profile. We plotted the maximum stretching force against the stretching distance for the three types of force profiles that resulted in nucleation (Figure 5). In the case of the WLC profile, the maximum stretching force varied from 120 pN to 600 pN and its stretching length was mostly shorter than L_c of a single SELP. For the sawtooth profile, the maximum stretching force was in a similar range, yet ~30% of the profiles had the stretch length beyond L_c, indicating that dimeric or trimeric species may be involved. Consistent with this, the number of peaks in a sawtooth profiles (2 to 14) can be more than twice the number of silk-elastin subunits in a SELP molecule, six. As mentioned above, exponential profiles have higher maximum stretching force (335 pN to 1200 pN) and stretching length (150 nm to 1 μm), again indicating involvement of a network of SELP molecules. The higher stretching force is consistent with a previous work showing that proteins in aggregating state has greater adhesion force than those in nonaggregating state.[39]

The likelihood of nucleation depended significantly on force profiles. Among all WLC profiles that we analyzed, only ~10% successfully led to nucleation. Since nucleation requires cooperation among multiple molecules, it is expected that stretching a single SELP is not a strong driver for nucleation, although surface diffusion of other chains and ordering around a stretched SELP may lead to nucleation. By contrast, the sawtooth and exponential profiles showed over 30% chance of nucleation.

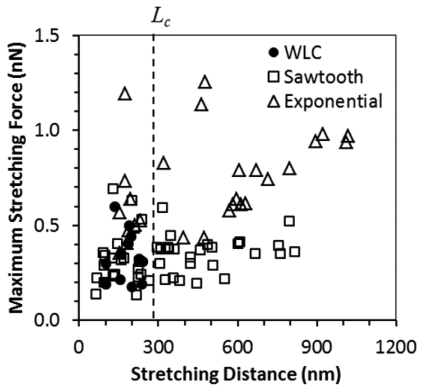

Figure 5. Maximum stretching force *vs* stretching distance of the three characteristic lateral force profiles.

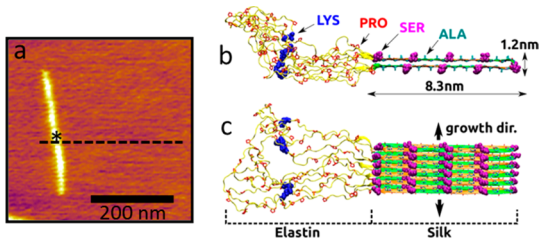

Figure 6. Single nanofiber pattern generated using time-lapse LFM. (a) Dotted line represents the single scan line location that induced nucleation. Once nucleation is detected (marked by asterisk), a larger area was scanned to confirm growth of amyloid perpendicular to the scan direction. (b, c) Atomistic model of a hairpin-like β-sheet bilayer structure of SELP. Axial view (b) and top view (c).

Whereas the WLC profile may reflect pulling a single SELP molecule in a random coil state, the sawtooth profile may be for one or two SELP molecules partially ordered and form β-sheets. In the case of Aβ1-40, it has also been suggested that prefibrillar aggregates contain ordered β-sheets.[40] SELP containing locally ordered β-sheets may be in a kinetically trapped state, where pulling and sequential unraveling of the disordered regions as in the sawtooth profiles may assist with finding a higher ordered state, leading to nucleation. After stretched domains are released, they can quickly rearrange as the chain is detached and relaxed from the tip.[41]

For exponential profiles, 60% of cases led to nucleation. Since multiple SELP molecules form a network, stretching them in one direction will enhance the likelihood for nearby domains to form β-sheets, similar to a mechanism demonstrated computationally.[42] It is likely that silk blocks are mainly responsible for kinetically trapped state. Another type of SELP that contains four blocks of silk unit and the same number of elastin blocks formed nanofibers instantaneously on mica,[24] whereas the SELP used in the present study, having eight silk blocks, took days to grow.[25] This indicates that the high content of the silk unit in SELP tends to stabilize kinetically trapped states on the surface, hence preventing amyloid nucleation without external force stimulus.

To test dependence of nucleation on the SELP concentration, we tested a 100× diluted solution (0.05 μg/mL). Under the same scanning condition, neither exponential profiles nor nucleation of fibers were observed, and the frequency of WLC behavior increased relative to the sawtooth behavior (Supporting Information Figure 4). This suggests that at this lower concentration, pulling occurs mostly on a single SELP molecule and is less likely to lead to nucleation since there are not enough molecules around the stretched SELP to support further growth. Also, at 5 μg/mL, the overall frequency of nucleation decreased with scan time, which is presumably due to less availability of SELP monomers as more nanofibers grow (Supporting Information Figure 5).

Mechanism for Force Induced Nucleation. Macroscopic agitation such as sonication on mature amyloid fibers can also break them, so that the fragments serve as seeds for further growth of nanofibers.[10] In other systems, sonication that provides random mechanical force resulted in acceleration of amyloid formation by reducing a lag phase or by forming aggregated structure, not by fragmentation of pre-existing fibrils.[43,44] Shear flow was also shown to induce aggregation and amyloid nucleation.[45−47] Recently, it was found that moderate levels of shear can trigger coil-to-β sheet transition presumably by stretching a polypeptide macromolecule.[48,49] In a related vein, elongational flow was speculated as one of the major mechanisms of ordering in the spinning apparatus of the silkworm.[50]

At the level of individual filaments, a previous report showed that tapping by AFM can break amyloid nanofibers on a mica surface, creating fragments which can serve as nuclei for new amyloid growth.[51] The present study shows another mechanism by which mechanical pulling of a molecule bypasses a high energy barrier for nucleation and initiates assembly. Our results indicate that macroscopic shear force or sonication may play a similar role where the extended molecule provides a template on which a β-sheet can form and propagate, effectively lowering the activation energy for nucleation. Recently, it was shown that mechanical manipulation of nanofiber creates active surfaces where a new nanofilament grows epitaxially by lattice matching.[52] This study used a 9-residue peptide that consists of mostly nonpolar residues. Because of its small size and weak binding, the filament can easily rotate and align with the hexagonal mica lattice.[53] In the case of SELP, its large size (842 residues) makes the resulting filament difficult to align with the mica lattice, and the randomly oriented filament network can form on the surface.[24] This allows the SELP fiber to grow perpendicular to the scanning direction irrespective of the orientation relative to the underlying mica lattice.[25]

In general, the lateral force originates from instantaneous bond formation and breakage between two objects moving relative to each other (chemical friction).[54] In the AFM experiments on polymer films, including those of proteins, elastomers, and synthetic

polymers,[55] lateral force can arise from the stretching of protruded chain segments, which causes sawtooth patterns in lateral force profiles.[56] Plowing[57] and dragging on the surface[58] can also increase lateral force. In our case, no accumulation of SELP was observed at edges of the scanned area, indicating that plowing and dragging do not play any major role. The lateral force profiles fitted with a WLC model show that SELP with these profiles is largely unstructured like the PEVK region in titin.[59] Lack of any strong correlation between the location of nuclei and where the stretching starts suggests that nuclei can form at any part along the stretched molecules. Weak bonds that break and cause the sawtooth profile during stretching are called sacrificial bonds.[37] They can reform reversibly, thereby providing a "self-healing" nature to the material. Similar force levels and the relatively uniform periodicity of the peaks indicate that partially ordered silk units are likely to be responsible for this behavior. The increased probability of nucleation in these force profiles indicates that breaking of sacrificial bonds allows rapid conformational rearrangement to form β hairpin structures.

The exponential force profiles showed the highest probability (60%) of nucleation. This force profile has been observed in both capture-silk molecules and intact strands of the capture silk.[38] As mentioned above, different force profiles may arise from responses of different molecular species, where WLC corresponds to a single or a few SELP molecules in disordered states, sawtooth to partially ordered SELP molecules, and the exponential profile to a network of SELP molecules containing locally ordered domains. In the exponential case, stretching of the network will provide a significant advantage in nucleation *via* multiple intermolecular interactions in an extended conformation. A high resolution *in situ* AFM study of self-assembly revealed multiple oligomeric species involved in dynamic assembly and disassembly process of amelogenin on surfaces.[60] We speculate that the different force profiles may indicate heterogeneous populations of SELP oligomers on the surface.

We have previously achieved micrometer scale pattern composed of multiple nanofibers in AFM tapping mode.[26] However, controlled generation of single nanofibers has been challenging, as scanning of smaller areas did not lead to nucleation. In the present study, after revealing the molecular level mechanism of nucleation, time-lapse LFM was applied to create a single nanofiber pattern with directional control. A single line scan (Figure 6a, dotted line) was continuously performed until a single nucleation (Figure 6a, asterisk) is created in the height profile. Immediately after the nucleation, the line scan was stopped and a larger area was imaged. Indeed, a single nanofiber grew from the induced nuclei oriented almost perpendicular to the scan direction.

On the basis of our measurements, we constructed a tentative structural model for the SELP amyloid as a hairpin-like β-sheet bilayer (Figure 6b), which has also been previously speculated.[49] The two facing β-sheets are likely held together by van der Waals interactions, where stabilization is provided by hydrophobic interactions.[61] The width of the amyloid core in this model is 8.3 nm, which is close to the value measured using a sharpened tip with 2 nm of nominal radius of curvature and support the involvement of the silk unit in forming the cross-β structure. In contrast, since prolines are strong β-sheet breakers,[62] the proline-rich elastin unit likely protrudes from the side of the cross-β core, and possibly wraps around it. The elastin unit also provides a linkage between two amyloid cores, which may be involved with the secondary nucleation event next to the first nucleation site. Assembly of additional strands results in the growth of the amyloid fiber (Figure 6c).

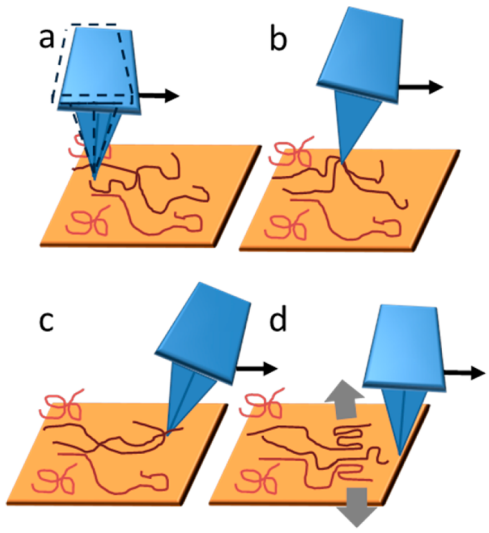

Figure 7. Proposed mechanism for mechanically induced amyloid nucleation. (a) As the tip moves along a scan line, it twists due to the frictional force with the SELP-coated surface. (b) A SELP oligomer is attached to the tip, increasing lateral force during the scan. (c) As the oligomeric SELP is stretched, individual SELP molecules align to the scan direction. The extended conformation of SELP serves as a template for nucleation by incorporating nearby SELP molecules. (d) SELP detaches from the tip and amyloid fiber elongates perpendicular to the stretching direction.

The adsorbed SELP is likely to have a reduced number of conformational states, thereby reducing the entropic cost of folding on the surface compared to the bulk case. It is expected that there is limited surface diffusion of SELP, which facilitates local oligomerization. The oligomerized state may form during the line scan as well. When SELP is mechanically stretched by the AFM tip, its extended conformation allows other molecules to assemble onto it, forming nuclei (Figure 7), which is akin to the induced-fit mechanism.[63] After a SELP is detached from the tip, it may further accelerate nucleation by interacting with the aligned oligomeric state. The orientation of the nanofiber is governed by the stretching direction. This

stretching by AFM is analogous to the action of the regulatory protein chaperone that reverses a misfolded protein intermediate to its native state by mechanical pulling.[64]

CONCLUSIONS

Our measurements reveal a direct correlation between molecular stretching and amyloid nucleation. The fact that the fiber growth direction is perpendicular to stretching implies that the stretched state provides templates that determine the growth direction. Using this technique, a single nanofiber pattern was successfully created. Insights learned from the present study may contribute to developing novel strategies for mechanically guiding self-assembly of peptide nanofibers.

METHODS

Sample Preparation. Silk-elastin-like protein polymer (SELP) is composed of specific repeating amino acids from *Bombyx mori* (silkworm) silk (Gly-Ala-Gly-Ala-Gly-Ser) and mammalian elastin (Gly-Val-Gly-Val-Pro) and is produced using DNA recombinant technology.[22] One SELP unit consists of 8 *Bombyx mori* silk-like (GAGAGS), 15 elastin-like (GVGVP), and one lysine-modified elastin-like (GKGVP) blocks. One polymer chain consists of a head, six SELP units, and a tail. The molecular weight is 65 374 Da and its complete amino acid sequence is MDPVVLQRRDWENPGVTQLNRLAAHPPFASDPM**[GAGS(GAGAGS)$_2$(GVGVP)$_4$-GKGVP(GVGVP)$_{11}$(GAGAGS)$_5$GAGA]$_6$**MDPGRYQDLRSHHHHHH. A 40 μL aliquot of 5 μg/mL SELP in distilled water was dropped on a freshly cleaved mica disk (Ted Pella, Inc., CA). Samples were incubated for 30 min in a humidity chamber at room temperature and then washed with distilled water three times. All AFM images and lateral force measurements were obtained in distilled water.

Time-Lapse Lateral Force Microscopy. Time-lapse LFM experiments were performed using the Molecular Force Probe-3D instrument (MFP-3D, Asylum Research, CA) to obtain height profiles and lateral force profiles simultaneously. A rectangular silicon nitride probe (MLCT, Bruker, CA) was used. The spring constant (17 pN/nm) in the normal direction was obtained using thermal tuning method. The lateral sensitivity was determined using the wedge calibration method[65,66] and ranged from 100 to 250 pN/mV. The normal force was 140 pN during the lateral scan, which ensured occasional increases in lateral forces, hence nucleation events. The SELP modified tip was prepared by scanning an AFM tip on SELP adsorbed mica surface. The initial lateral force was ~1 nN and it decreased to ~150 pN after several scans, indicating that SELP is adsorbed to the AFM tip. The background lateral force exerted between the SELP-modified tip and the SELP-adsorbed mica was 165 $\pm$ 89 pN (n = 12). The lateral force is positive during trace (left to right) and negative during retrace (right to left). Time-lapse experiment was carried out in "slow-scan disabled" mode where the same scan line with 2-μm width was repeatedly scanned as a function of time. Hence the images from time-lapse experiments are time series of height trajectories from a single scan line. The scan frequency was 2 Hz, providing time resolution of 0.25 s per scan line. High resolution AFM imaging was performed using a silicon tip (MSNL, Bruker, CA) with a nominal tip radius of 2 nm. To provide force−extension behaviors of a single SELP molecule, we also stretched the SELP molecule normal to the mica surface, as described in our previous work.[67]

Data Analysis. Height of the nucleus was determined from peak-to-peak distance in Gaussian fits of the time series data for the baseline and for the new nucleation site. The histogram of nucleation heights was also fit by multiple Gaussian functions to obtain step sizes in height increase. The maximum stretching force in the lateral force profile was defined as the difference between the maximum peak force and the background lateral force. For sawtooth profiles, the average peak forces were used as the maximum stretching force. The width of the nucleus was obtained from a full width at half-maximum value from Gaussian fit of the height profile. WLC and exponential fits to lateral force profiles were done using the least-squares likelihood estimation method. Normal force profiles for single-molecule stretching experiments were also fit using the WLC model, which produced L_p = 0.28 $\pm$ 0.10 nm and L_c = 284 $\pm$ 13 nm (n = 64) (see Supporting Information, Figure 3).

Atomic Model. All modeling and simulation were carried out using the CHARMM program[68] with the param19 force field.[69] Because of the similarity in the length of Aβ1-42 and the silk part, $(GAGAGS)_8$, we modeled the amyloid core of SELP based on the solid-state NMR structure of Aβ1-42 (Protein Data Bank ID: 2BEG).[33] The backbone of PDB 2BEG was used to make the silk part into a hairpin-like β-strand. After generating the β-sheet filament, the system was briefly energy minimized to allow backbone hydrogen bond formation between neighboring strands. To build the elastin domain, the N- and C-terminal half strands were generated in extended configuration, which were respectively joined to the termini of the silk part. The other ends of the two half strands were connected by using the ModLoop utility[70] in the Modeller program.[71] We carried out additional energy minimization after building the full SELP amyloid, then carried out molecular dynamics simulation with backbone heavy atoms of the silk amyloid core harmonically restrained, with a spring constant of 5 kcal/mol·Å^2. The main purpose of this simulation was to relax the elastin part. The simulation was performed with a 2-fs integration step, for 2 ns at 600 K, in the EEF1 implicit solvent environment of CHARMM.[72] The resulting structures are shown in Figure 6b,c.

Conflict of Interest: The authors declare no competing financial interest.

Acknowledgment. J. S. and S.D.S. gratefully acknowledge support from the U.S. National Science Foundation *via* award No. DMR-1056552 and CMMI-0841840, respectively. We also acknowledge the support of the Maryland NanoCenter.

Supporting Information Available: Five figures. (Figure 1) AFM image of adsorbed SELP layer on mica; (Figure 2) stepwise height increase during amyloid nucleation; (Figure 3) force *vs* distance profile obtained during stretching a SELP molecule perpendicular to the mica surface. (Figure 4) effect of SELP concentration on percentages of three force profiles; (Figure 5) frequency of nucleation as a function of scan time for the three force profiles. This material is available free of charge *via* the Internet at http://pubs.acs.org.

REFERENCES AND NOTES

1. Dobson, C. M. Protein Folding and Misfolding. *Nature* **2003**, *426*, 884–890.
2. Nelson, R.; Sawaya, M. R.; Balbirnie, M.; Madsen, A. O.; Riekel, C.; Grothe, R.; Eisenberg, D. Structure of the Cross-β Spine of Amyloid-like Fibrils. *Nature* **2005**, *435*, 773–778.
3. Fandrich, M.; Dobson, C. M. The Behaviour of Polyamino Acids Reveals an Inverse Side Chain Effect in Amyloid Structure Formation. *EMBO J.* **2002**, *21*, 5682–5690.
4. Jarrett, J. T.; Berger, E. P.; Lansbury, P. T., Jr. The Carboxy Terminus of the β Amyloid Protein is Critical for the Seeding of Amyloid Formation: Implications for the Pathogenesis of Alzheimer's Disease. *Biochemistry* **1993**, *32*, 4693–4697.
5. Nielsen, L.; Khurana, R.; Coats, A.; Frokjaer, S.; Brange, J.; Vyas, S.; Uversky, V. N.; Fink, A. L. Effect of Environmental Factors on the Kinetics of Insulin Fibril Formation: Elucidation of the Molecular Mechanism. *Biochemistry* **2001**, *40*, 6036–6046.
6. Abrahamson, M.; Grubb, A. Increased Body Temperature Accelerates Aggregation of the Leu-68→Gln Mutant Cystatin C, the Amyloid-Forming Protein in Hereditary

Cystatin C Amyloid Angiopathy. *Proc. Natl. Acad. Sci. U.S.A.* **1994**, *91*, 1416–1420.
7. Merlini, G.; Bellotti, V. Molecular Mechanisms of Amyloidosis. *New Engl. J. Med.* **2003**, *349*, 583–596.
8. Teplow, D. B.; Lazo, N. D.; Bitan, G.; Bernstein, S.; Wyttenbach, T.; Bowers, M. T.; Baumketner, A.; Shea, J. E.; Urbanc, B.; Cruz, L.; *et al.* Elucidating Amyloid β-Protein Folding and Assembly: A Multidisciplinary Approach. *Acc. Chem. Res.* **2006**, *39*, 635–645.
9. Kodali, R.; Wetzel, R. Polymorphism in the Intermediates and Products of Amyloid Assembly. *Curr. Opin. Struct. Biol.* **2007**, *17*, 48–57.
10. Petkova, A. T.; Leapman, R. D.; Guo, Z.; Yau, W. M.; Mattson, M. P.; Tycko, R. Self-Propagating, Molecular-Level Polymorphism in Alzheimer's β-Amyloid Fibrils. *Science* **2005**, *307*, 262–265.
11. Kowalewski, T.; Holtzman, D. M. *In Situ* Atomic Force Microscopy Study of Alzheimer's β-Amyloid Peptide on Different Substrates: New Insights into Mechanism of β-Sheet Formation. *Proc. Natl. Acad. Sci. U.S.A.* **1999**, *96*, 3688–3693.
12. Zhu, M.; Souillac, P. O.; Ionescu-Zanetti, C.; Carter, S. A.; Fink, A. L. Surface-Catalyzed Amyloid Fibril Formation. *J. Biol. Chem.* **2002**, *277*, 50914–50922.
13. Hoyer, W.; Cherny, D.; Subramaniam, V.; Jovin, T. M. Rapid Self-Assembly of α-Synuclein Observed by *in Situ* Atomic Force Microscopy. *J. Mol. Biol.* **2004**, *340*, 127–139.
14. McMasters, M. J.; Hammer, R. P.; McCarley, R. L. Surface-Induced Aggregation of β Amyloid Peptide by Omega-Substituted Alkanethiol Monolayers Supported on Gold. *Langmuir* **2005**, *21*, 4464–4470.
15. Ha, C.; Park, C. B. *Ex Situ* Atomic Force Microscopy Analysis of β-Amyloid Self-Assembly and Deposition on a Synthetic Template. *Langmuir* **2006**, *22*, 6977–6985.
16. Nayak, A.; Dutta, A. K.; Belfort, G. Surface-Enhanced Nucleation of Insulin Amyloid Fibrillation. *Biochem. Biophys. Res. Commun.* **2008**, *369*, 303–307.
17. Arimon, M.; Diez-Perez, I.; Kogan, M. J.; Durany, N.; Giralt, E.; Sanz, F.; Fernandez-Busquets, X. Fine Structure Study of Aβ1-42 Fibrillogenesis with Atomic Force Microscopy. *FASEB J.* **2005**, *19*, 1344–1346.
18. Kellermayer, M. S.; Karsai, A.; Benke, M.; Soos, K.; Penke, B. Stepwise Dynamics of Epitaxially Growing Single Amyloid Fibrils. *Proc. Natl. Acad. Sci. U.S.A.* **2008**, *105*, 141–144.
19. Brown, C. L.; Aksay, I. A.; Saville, D. A.; Hecht, M. H. Template-Directed Assembly of a *de Novo* Designed Protein. *J. Am. Chem. Soc.* **2002**, *124*, 6846–6848.
20. Yang, H.; Fung, S. Y.; Pritzker, M.; Chen, P. Surface-Assisted Assembly of an Ionic-Complementary Peptide: Controllable Growth of Nanofibers. *J. Am. Chem. Soc.* **2007**, *129*, 12200–12210.
21. Geisler, M.; Xiao, S.; Puchner, E. M.; Grater, F.; Hugel, T. Controlling the Structure of Proteins at Surfaces. *J. Am. Chem. Soc.* **2010**, *132*, 17277–17281.
22. Dandu, R.; Von Cresce, A.; Briber, R.; Dowell, P.; Cappello, J.; Ghandehari, H. Silk-Elastinlike Protein Polymer Hydrogels: Influence of Monomer Sequence on Physicochemical Properties. *Polymer* **2009**, *50*, 366–374.
23. Gosline, J.; Lillie, M.; Carrington, E.; Guerette, P.; Ortlepp, C.; Savage, K. Elastic Proteins: Biological Roles and Mechanical Properties. *Philos. Trans. R. Soc. London, B: Biol. Sci.* **2002**, *357*, 121–132.
24. Hwang, W.; Kim, B. H.; Dandu, R.; Cappello, J.; Ghandehari, H.; Seog, J. Surface Induced Nanofiber Growth by Self-Assembly of a Silk-Elastin-like Protein Polymer. *Langmuir* **2009**, *25*, 12682–12686.
25. Chang, J.; Peng, X. F.; Hijji, K.; Cappello, J.; Ghandehari, H.; Solares, S. D.; Seog, J. Nanomechanical Stimulus Accelerates and Directs the Self-Assembly of Silk-Elastin-like Nanofibers. *J. Am. Chem. Soc.* **2011**, *133*, 1745–1747.
26. Johnson, S.; Ko, Y. K.; Varongchayakul, N.; Lee, S.; Cappello, J.; Ghandehari, H.; Lee, S. B.; Solares, S. D.; Seog, J. Directed Patterning of the Self-Assembled Silk-Elastin-like Nanofibers Using a Nanomechanical Stimulus. *Chem. Commun.* **2012**, *48*, 10654–10656.
27. Lashuel, H. A.; Hartley, D.; Petre, B. M.; Walz, T.; Lansbury, P. T., Jr. Neurodegenerative Disease: Amyloid Pores from Pathogenic Mutations. *Nature* **2002**, *418*, 291.
28. Mastrangelo, I. A.; Ahmed, M.; Sato, T.; Liu, W.; Wang, C.; Hough, P.; Smith, S. O. High-Resolution Atomic Force Microscopy of Soluble Aβ42 Oligomers. *J. Mol. Biol.* **2006**, *358*, 106–119.
29. Dai, B.; Kang, S. G.; Huynh, T.; Lei, H. Z.; Castelli, M.; Hu, J.; Zhang, Y.; Zhou, R. H. Salts Drive Controllable Multilayered Upright Assembly of Amyloid-like Peptides at Mica/Water Interface. *Proc. Natl. Acad. Sci. U.S.A.* **2013**, *110*, 8543–8548.
30. Kang, S. G.; Huynh, T.; Xia, Z.; Zhang, Y.; Fang, H. P.; Wei, G. H.; Zhou, R. H. Hydrophobic Interaction Drives Surface-Assisted Epitaxial Assembly of Amyloid-like Peptides. *J. Am. Chem. Soc.* **2013**, *135*, 3150–3157.
31. Petkova, A. T.; Ishii, Y.; Balbach, J. J.; Antzutkin, O. N.; Leapman, R. D.; Delaglio, F.; Tycko, R. A Structural Model for Alzheimer's β-Amyloid Fibrils Based on Experimental Constraints from Solid State NMR. *Proc. Natl. Acad. Sci. U.S. A.* **2002**, *99*, 16742–16747.
32. Paravastu, A. K.; Leapman, R. D.; Yau, W. M.; Tycko, R. Molecular Structural Basis for Polymorphism in Alzheimer's β-amyloid Fibrils. *Proc. Natl. Acad. Sci. U.S.A.* **2008**, *105*, 18349–18354.
33. Luhrs, T.; Ritter, C.; Adrian, M.; Riek-Loher, D.; Bohrmann, B.; Dobeli, H.; Schubert, D.; Riek, R. 3D Structure of Alzheimer's Amyloid-β(1-42) Fibrils. *Proc. Natl. Acad. Sci. U.S.A.* **2005**, *102*, 17342–17347.
34. Lazo, N. D.; Grant, M. A.; Condron, M. C.; Rigby, A. C.; Teplow, D. B. On the Nucleation of Amyloid β-Protein Monomer Folding. *Protein Sci.* **2005**, *14*, 1581–1596.
35. Marko, J. F.; Siggia, E. D. Stretching DNA. *Macromolecules* **1995**, *28*, 8759–8770.
36. Urry, D. W.; Hugel, T.; Seitz, M.; Gaub, H. E.; Sheiba, L.; Dea, J.; Xu, J.; Parker, T. Elastin: a Representative Ideal Protein Elastomer. *Philos. Trans. R. Soc. London, B: Biol. Sci.* **2002**, *357*, 169–184.
37. Fantner, G. E.; Oroudjev, E.; Schitter, G.; Golde, L. S.; Thurner, P.; Finch, M. M.; Turner, P.; Gutsmann, T.; Morse, D. E.; Hansma, H.; et al. Sacrificial Bonds and Hidden Length: Unraveling Molecular Mesostructures in Tough Materials. *Biophys. J.* **2006**, *90*, 1411–1418.
38. Becker, N.; Oroudjev, E.; Mutz, S.; Cleveland, J. P.; Hansma, P. K.; Hayashi, C. Y.; Makarov, D. E.; Hansma, H. G. Molecular Nanosprings in Spider Capture-Silk Threads. *Nat. Mater.* **2003**, *2*, 278–283.
39. McAllister, C.; Karymov, M. A.; Kawano, Y.; Lushnikov, A. Y.; Mikheikin, A.; Uversky, V. N.; Lyubchenko, Y. L. Protein Interactions and Misfolding Analyzed by AFM Force Spectroscopy. *J. Mol. Biol.* **2005**, *354*, 1028–1042.
40. Chimon, S.; Ishii, Y. Capturing Intermediate Structures of Alzheimer's β-Amyloid, Aβ(1-40), by Solid-State NMR Spectroscopy. *J. Am. Chem. Soc.* **2005**, *127*, 13472–13473.
41. Rief, M.; Gautel, M.; Oesterhelt, F.; Fernandez, J. M.; Gaub, H. E. Reversible Unfolding of Individual Titin Immunoglobulin Domains by AFM. *Science* **1997**, *276*, 1109–1112.
42. Keten, S.; Buehler, M. J. Nanostructure and Molecular Mechanics of Spider Dragline Silk Protein Assemblies. *J. R. Soc. Interface* **2010**, *7*, 1709–1721.
43. So, M.; Yagi, H.; Sakurai, K.; Ogi, H.; Naiki, H.; Goto, Y. Ultrasonication-Dependent Acceleration of Amyloid Fibril Formation. *J. Mol. Biol.* **2011**, *412*, 568–577.
44. Stathopulos, P. B.; Scholz, G. A.; Hwang, Y. M.; Rumfeldt, J. A.; Lepock, J. R.; Meiering, E. M. Sonication of Proteins Causes Formation of Aggregates That Resemble Amyloid. *Protein Sci.* **2004**, *13*, 3017–3027.
45. Loksztejn, A.; Dzwolak, W. Vortex-Induced Formation of Insulin Amyloid Superstructures Probed by Time-Lapse Atomic Force Microscopy and Circular Dichroism Spectroscopy. *J. Mol. Biol.* **2010**, *395*, 643–655.
46. Lee, J. S.; Ryu, J.; Park, C. B. High-Throughput Analysis of Alzheimer's β-Amyloid Aggregation Using a Microfluidic Self-Assembly of Monomers. *Anal. Chem.* **2009**, *81*, 2751–2759.

47. Hill, E. K.; Krebs, B.; Goodall, D. G.; Howlett, G. J.; Dunstan, D. E. Shear Flow Induces Amyloid Fibril Formation. *Biomacromolecules* **2006**, *7*, 10–13.
48. Ohgo, K.; Bagusat, F.; Asakura, T.; Scheler, U. Investigation of Structural Transition of Regenerated Silk Fibroin Aqueous Solution by Rheo-NMR Spectroscopy. *J. Am. Chem. Soc.* **2008**, *130*, 4182–4186.
49. Gong, Z.; Huang, L.; Yang, Y.; Chen, X.; Shao, Z. Two Distinct β-Sheet Fibrils from Silk Protein. *Chem. Commun.* **2009**, 7506–7508.
50. Vollrath, F.; Knight, D. P. Liquid Crystalline Spinning of Spider Silk. *Nature* **2001**, *410*, 541–548.
51. Yang, H.; Fung, S. Y.; Pritzker, M.; Chen, P. Mechanical–Force–Induced Nucleation and Growth of Peptide Nanofibers at Liquid/Solid Interfaces. *Angew. Chem.* **2008**, *120*, 4469–4472.
52. Zhang, F. C.; Zhang, F.; Su, H. N.; Li, H.; Zhang, Y.; Hu, J. Mechanical Manipulation Assisted Self-Assembly to Achieve Defect Repair and Guided Epitaxial Growth of Individual Peptide Nanofilaments. *ACS Nano* **2010**, *4*, 5791–5796.
53. Leow, W. W.; Hwang, W. Epitaxially Guided Assembly of Collagen Layers on Mica Surfaces. *Langmuir* **2011**, *27*, 10907–10913.
54. Frisbie, C. D.; Rozsnyai, L. F.; Noy, A.; Wrighton, M. S.; Lieber, C. M. Functional Group Imaging by Chemical Force Microscopy. *Science* **1994**, *265*, 2071–2074.
55. Maeda, N.; Chen, N. H.; Tirrell, M.; Israelachvili, J. N. Adhesion and Friction Mechanisms of Polymer-on-Polymer Surfaces. *Science* **2002**, *297*, 379–382.
56. Overney, R. M.; Meyer, E.; Frommer, J.; Guntherodt, H. J.; Fujihira, M.; Takano, H.; Gotoh, Y. Force Microscopy Study of Friction and Elastic Compliance of Phase-Separated Organic Thin-Films. *Langmuir* **1994**, *10*, 1281–1286.
57. Holmberg, K.; Ronkainen, H.; Laukkanen, A.; Wallin, K. Friction and Wear of Coated Surfaces-Scales, Modelling and Simulation of Tribomechanisms. *Surf. Coat. Technol.* **2007**, *202*, 1034–1049.
58. Bo, Z.; Peng, X.; Chun-Lei, W.; Hai-Ping, F. Peptide Friction in Water Nanofilm on Mica Surface. *Chin. Phys. B* **2012**, *21*, 026801.
59. Li, H.; Linke, W. A.; Oberhauser, A. F.; Carrion-Vazquez, M.; Kerkvliet, J. G.; Lu, H.; Marszalek, P. E.; Fernandez, J. M. Reverse Engineering of the Giant Muscle Protein Titin. *Nature* **2002**, *418*, 998–1002.
60. Chen, C. L.; Bromley, K. M.; Moradian-Oldak, J.; DeYoreo, J. J. *In situ* AFM Study of Amelogenin Assembly and Disassembly Dynamics on Charged Surfaces Provides Insights on Matrix Protein Self-Assembly. *J. Am. Chem. Soc.* **2011**, *133*, 17406–17413.
61. Park, J.; Kahng, B.; Hwang, W. Thermodynamic Selection of Steric Zipper Patterns in the Amyloid Cross-β Spine. *PLoS Comput. Biol.* **2009**, *5*, e1000492.
62. Li, S. C.; Goto, N. K.; Williams, K. A.; Deber, C. M. Alpha-Helical, but not β-Sheet, Propensity of Proline is Determined by Peptide Environment. *Proc. Natl. Acad. Sci. U.S.A.* **1996**, *93*, 6676–6681.
63. Dong, J.; Wan, Z. L.; Popov, M.; Carey, P. R.; Weiss, M. A. Insulin Assembly Damps Conformational Fluctuations: Raman Analysis of Amide I Linewidths in Native States and Fibrils. *J. Mol. Biol.* **2003**, *330*, 431–442.
64. Todd, M. J.; Lorimer, G. H.; Thirumalai, D. Chaperonin-Facilitated Protein Folding: Optimization of Rate and Yield by an Iterative Annealing Mechanism. *Proc. Natl. Acad. Sci. U.S.A.* **1996**, *93*, 4030–4035.
65. Ogletree, D. F.; Carpick, R. W.; Salmeron, M. Calibration of Frictional Forces in Atomic Force Microscopy. *Rev. Sci. Instrum.* **1996**, *67*, 3298–3306.
66. Varenberg, M.; Etsion, I.; Halperin, G. An Improved Wedge Calibration Method for Lateral Force in Atomic Force Microscopy. *Rev. Sci. Instrum.* **2003**, *74*, 3362–3367.
67. Chung, J. W.; Shin, D.; Kwak, J. M.; Seog, J. Direct Force Measurement of Single DNA-Peptide Interactions Using Atomic Force Microscopy. *J. Mol. Recognit.* **2013**, *26*, 268–275.
68. Brooks, B. R.; Brooks, C. L., 3rd; Mackerell, A. D., Jr.; Nilsson, L.; Petrella, R. J.; Roux, B.; Won, Y.; Archontis, G.; Bartels, C.; Boresch, S.; *et al*. CHARMM: the Biomolecular Simulation Program. *J. Comput. Chem.* **2009**, *30*, 1545–1614.
69. Neria, E.; Fischer, S.; Karplus, M. Simulation of Activation Free Energies in Molecular Systems. *J. Chem. Phys.* **1996**, *105*, 1902–1921.
70. Fiser, A.; Sali, A. ModLoop: Automated Modeling of Loops in Protein Structures. *Bioinformatics* **2003**, *19*, 2500–2501.
71. Marti-Renom, M. A.; Stuart, A. C.; Fiser, A.; Sanchez, R.; Melo, F.; Sali, A. Comparative Protein Structure Modeling of Genes and Genomes. *Annu. Rev. Biophys. Biomol. Struct.* **2000**, *29*, 291–325.
72. Lazaridis, T.; Karplus, M. Effective Energy Function for Proteins in Solution. *Proteins* **1999**, *35*, 133–152.